LUND UNIVERSITY
Faculty of Science

Investigating the *GW* self-energy of the homogeneous electron gas in real space

Zhen Zhao

Thesis submitted for the degree of Master of Science
Project duration: 4 months

Supervised by Ferdi Aryasetiawan

Department of Physics
Division of Mathematical Physics
May 2018

Abstract

The real space behavior of the GW self-energy in the electron gas model was investigated in this thesis work. The self-energy is naturally decomposed into the screened-exchange and the Coulomb-hole components. The self-energy calculated with different electron densities as function of frequency and position was compared with the static approximation. At low frequency, the screened-exchange self-energy is highly localized and can be well approximated by the static approximation. It can also be well approximated by an exchange potential with a Yukawa interaction characterized in range by the Fermi momentum. The Coulomb-hole self-energy shows a strong dependence on frequency and can be repulsive over a certain region of space at low density. The total self-energy is localized within the Wigner-Seitz radius and the degree of localization increases with decreasing density. The results of the present work may serve as a guidance for constructing an approximate self-energy in real materials.

Contents

List of Figures

List of acronyms

HA Hartree approximation

HFA Hartree-Fock approximation

DFT Density Functional Theory

KS Kohn Sham

LDA Local-density approximation

GWA *GW* approximation

SEX Screened-exchange

COH Coulomb-hole

1 Introduction

Many physical properties in condensed matter physics arise from the Coulomb interaction among the electrons. Were it not for this interaction we would not observe fascinating phenomena such as colossal magneto resistance, which has been utilized in our computer hard disks, superconductivity, magnetism in general, and numerous other phenomena. These phenomena are not only interesting from the point of view of scientific endeavor but also from technological point of view. Technological advances based on basic science have changed people's life in a fundamental fashion.

An important ingredient in determining physical properties of a material is its electronic structure, which in turn is governed by the Coulomb interaction among the electrons and the external potential in which the electrons move. The electronic structure can in principle be calculated by solving the Schrödinger equation. However, due to the presence of electron-electron interaction in the many-electron Hamiltonian it is in practice impossible to solve the exact Schrödinger equation directly, except for small systems containing a few electrons.

Therefore, various approximate methods have been developed to get the essential knowledge of the electronic structure. One of the first general methods for approximating the many-electron Hamiltonian is the mean-field method, in which the electrons are assumed to move independently in an average field arising from the external field and the field from the electrons themselves. The Hartree approximation (HA) is perhaps one of the earliest mean-field approximations [1]. This approximation, however, does not take into account fully the fermionic nature of the electrons. The Hartree-Fock approximation (HFA) incorporates the Fermi statistics of the electrons resulting in the additional exchange interaction on top of the Hartree potential [2]. Ironically, the HFA, which at first sight should be a better approximation than the HA, turns out to be a rather poor approximation for solids. The reason for this is due to the neglect of electron correlations, which tend to cancel the effects of exchange. On the other hand, the HFA is quite reasonable for small molecules in which electron correlations manifested in the screening phenomenon are relatively small compared to the exchange interaction. To remedy the problem with the HFA in solids, Slater introduced the $X\alpha$ method [3], which replaces the nonlocal exchange interaction by a local one and mimics the effects of correlations by adjusting the coefficient of the exchange potential . Although it is not *apriori* clear why this should improve the HFA, it did give a much more accurate electronic structure.

The early 1960's witnessed the arrival of density functional theory (DFT) [4, 5], a new theory that eventually revolutionized the field of electronic structure [6]. In this theory, as the name suggests, it is the electron density that plays the main role instead of the wave function. The ground-state electron density determines the external potential and hence the many-electron Hamiltonian so that all physical properties obtainable from the Hamiltonian are functionals of the electron density. This finding, interesting as it may be, gives no clue as to how to compute any physical quantity. The practical realization of DFT was achieved by the construction of the Kohn-Sham (KS) scheme [5] in which an auxiliary system of noninteracting electrons with the same ground-state density as that of

the true interacting system was introduced as a means to compute the electron density and subsequently the total energy of the interacting system [5]. Using the variational property of the total energy, a noninteracting Schrödinger equation, known as the KS equation, was derived from which the ground-state electron density and total energy could be calculated. While the KS scheme furnishes a practical way of computing the ground-state total energy, it does not strictly speaking yield the electronic structure as measured in photoemission experiments. The electronic structure is not a ground-state property but rather an excited-state property that lies beyond the realm of the KS scheme. Nevertheless it is common practice to interpret the KS eigenvalues as the electronic structure of the system under study.

A theoretically proper way of computing the electronic structure is provided by the Green function technique, which is tailored to describe physical processes involving removal and addition of a single electron or particle, the type of processes occurring in photoemission and inverse photoemission experiments designed to measure one-particle binding and excitation energies in crystals.

A key quantity in Green's function theory is the self-energy, which may be regarded as a nonlocal and energy-dependent potential. It seems physically sensible indeed that each electron should experience a different potential depending on its position and energy. Needless to say, it is not feasible to calculate the exact self-energy for a real crystal and a resort to approximation is unavoidable. A very successful approximation to the self-energy developed in the early 1960's (about the same time as DFT) is the GW method [7, 8]. It is derived from many-body perturbation theory and has been proven to give remarkably accurate results in real materials. One of its achievements is remedying the systematic underestimation of band gaps in semiconductors and insulators within the local density approximation (LDA) of DFT.

Despite its success, a serious computational hinder is faced when applying the GW approximation (GWA) to complex systems due to the large scale of the computations as the systems become increasingly large. One approach to overcome this hinder is to simplify the GW calculations without significantly reducing the quantitative predictive power of the method. The present thesis work is aimed in that direction. While the goal is not to develop a simplified scheme per se, it is meant to provide insights and clues for simplifying the GW calculations. With this in mind, we will investigate the behavior of the GW self-energy in the electron gas model in real space as a function of position and energy. In particular, the self-energy can be decomposed naturally into the so-called screened exchange and Coulomb-hole terms. Questions we would like to address are, for example: What is the range of the self-energy at low-energy relevant to physical applications? What kind of generic shape does the self-energy have? Answers to such questions can provide useful information for designing an approximate self-energy for real systems.

1.1 Many-Electron Systems

For many-electron systems, the Hamiltonian is given by,

$$\begin{aligned}\hat{H} &= \sum_i [-\frac{1}{2}\boldsymbol{\nabla}_i^2 + V(\boldsymbol{r}_i)] + \frac{1}{2}\sum_{i\neq j}\frac{1}{|\boldsymbol{r}_i - \boldsymbol{r}_j|} \\ &= \hat{T} + \hat{V}_{\text{ext}} + \hat{v},\end{aligned} \tag{1.1}$$

where we used atomic units ($\hbar = m = e = 1$). They are used throughout the thesis and the subscript i refers to the ith electron. The kinetic term, the external potential term and the Coulomb interaction term are represented by $\hat{T}$, $\hat{V}_{\text{ext}}$ and $\hat{v}$, respectively. The electrons are correlated with each other by the Coulomb interactions, which results in the complexity of the Hamiltonian. As mentioned before, it is this last term that gives rise to many fascinating phenomena in condensed matter physics and at the same time it is this term that makes the many-electron problem extremely difficult to solve. It is safe to say that solving the problem directly by diagonalizing the Hamiltonian is out of the question for a system consisting a large number of electrons such as solids. The goal of many-body theory is then to find an approximate method which allows us to extract relevant physical quantities of interest with sufficient accuracy that permits quantitative predictions. In the following a brief overview is given of the various approximate methods to solve the many-electron problem starting from the mean-field theory.

1.2 Mean field theory

1.2.1 The Hartree approximation

A straightforward way to solve the time-independent many-body Schrödinger equation is to replace the Coulomb interaction felt by each electron with an average static field, which is called the Hartree potential:

$$\hat{V}_H(\boldsymbol{r}) = \int d\boldsymbol{r'} v(\boldsymbol{r} - \boldsymbol{r'})\rho(\boldsymbol{r'}), \tag{1.2}$$

where $\rho(\boldsymbol{r})$ is the electron density.

Under the Hartree approximation, the many-body Hamiltonian is simplified to the single-particle Hamiltonian,

$$\hat{H}_{\text{Hartree}} = \hat{T} + \hat{V}_{\text{ext}} + \hat{V}_H, \tag{1.3}$$

which can be solved self-consistently,

$$\begin{aligned}\hat{H}_{\text{Hartree}}\phi_i &= \epsilon_i\phi_i \\ \rho &= \sum_i^{\text{occ}} |\phi_i|^2.\end{aligned} \tag{1.4}$$

The new density is then used to generate a new Hartree potential and so on. The many-electron wave function in the Hartree approximation is approximated by a product of the N lowest occupied orbitals:

$$\Psi(\boldsymbol{r}_1, ..., \boldsymbol{r}_N) = \phi_1(\boldsymbol{r}_1)...\phi_N(\boldsymbol{r}_N), \tag{1.5}$$

where N is the number of electrons for each spin channel (since the Hartree Hamiltonian does not depend on spin, the two spin channels are the same). The Hartree approximation is far from accurate and it is not normally used in band structure calculations. For solids, however, it is better than the Hartree-Fock approximation described below, due to a cancellation between exchange and correlations.

1.2.2 The Hatree-Fock approximation

In the Hartree theory, the fermionic property of electrons is not included automatically since the wave function obtained by solving (1.4) is not required to be anti-symmetric as can be seen in (1.5). The Hartree-Fock approximation takes into account the Fermi statistics of the electrons, fulfilling the Pauli exclusion principle. The many-electron wave function is approximated by a single Slater determinant:

$$\Psi(r_1, r_2, \cdots, r_N) = \begin{vmatrix} \phi_1(r_1) & \phi_1(r_2) & \cdots & \phi_1(r_N) \\ \phi_2(r_1) & \phi_2(r_2) & \cdots & \phi_2(r_N) \\ \vdots & \vdots & \ddots & \vdots \\ \phi_N(r_1) & \phi_N(r_2) & \cdots & \phi_N(r_N) \end{vmatrix}, \tag{1.6}$$

where $r = (\boldsymbol{r}, \sigma)$.

The Hartree-Fock approximation (HFA) is an extension of the Hartree approximation by adding a spin-dependent non-local exchange potential term. The Hartree-Fock equation is then

$$[h_0(r) + V_H(r)]\phi_k(r) + \int d^3r' V_X(r, r')\phi_k(r') = \epsilon_k \phi_k(r), \tag{1.7}$$

where $h_0 = \hat{T} + \hat{V}_{\text{ext}}$ and $V_X(r, r')$ is the exchange potential,

$$V_X(r, r') = -v(\boldsymbol{r} - \boldsymbol{r}')\rho_X(r, r'), \tag{1.8}$$

and $\rho_X(r, r')$ is the density matrix,

$$\rho_X(r, r') = \sum_k^{\text{occ}} \phi_k(r)\phi_k^*(r'). \tag{1.9}$$

The HF equation is derived by minimizing the total energy (the expectation value of the many-electron Hamiltonian) with respect to the orbitals in the single Slater determinant defining the HF many-electron wave function. It is to be noted that the exchange potential is spin dependent, implying that exchange interaction is only operative between electrons of the same spin.

The free electron gas can be used as an illustration. The set of free electron wave functions,

$$\phi_{\boldsymbol{k}}(\boldsymbol{r}) = \frac{1}{\sqrt{V}} e^{i\boldsymbol{k}\cdot\boldsymbol{r}}, \tag{1.10}$$

is inserted into the Hartree-Fock equation 1.7, and the corresponding Hartree-Fock energy eigenvalue is compared with the free-electron energy dispersion, as shown in figure 1. The HF dispersion is depressed from the free-electron dispersion, due to the negative exchange term so that the occupied bandwidth is enlarged by approximately a factor of 2. However, photoemission experiments on the alkalis (e.g., sodium, aluminium, etc.), whose valence electrons can be modeled by the uniform electron gas, indicate that the occupied band width is narrowed rather than widened, contrary to the HF prediction. Moreover, the dispersion has a logarithmic singularity at the Fermi momentum leading to an unphysical zero density of states at the Fermi level. The electron gas HF results illustrate the important role of electron correlations, which tend to compensate the effects of exchange and remove the unphysical logarithmic singularity in the dispersion at the Fermi momentum. For the electron gas, exchange is canceled to a large extent by correlations but for real materials the degree of cancellation is material dependent. It is therefore necessary to have a theoretical scheme which can take into account electron correlations reliably.

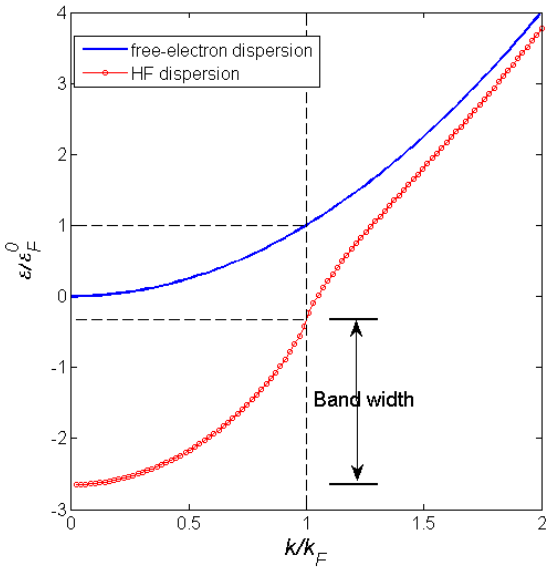

Figure 1: The Hartree-Fock energy dispersion (red line with dot mark) compared with the free electron dispersion (blue line), from [9]. The energy is in the unit of free-electron Fermi energy $\epsilon_F^0 = \frac{1}{2}k_F^2$. The HF occupied band width is approximately twice that of the corresponding free-electron value.

1.3 Density functional theory

1.3.1 The Hohenberg-Kohn theorem

The Hohenberg-Kohn theorem, put forward in 1964 [4], proves that the ground-state electron density determines the external potential uniquely. This theorem may be summarized by the following corollaries

- The first corollary: For a many-electron system, the expectation value of a ground state observable (such as the total energy of the system) is a functional of the ground-state electron density.
- The second corollary: the energy functional is minimal at the ground state density, and the minimum is equal to the ground state energy.

The total energy may be conventionally decomposed into the following components:

$$E[\rho] = T[\rho] + E_H[\rho] + E_{\text{ext}}[\rho] + E_{\text{xc}}[\rho], \tag{1.11}$$

where T is the kinetic energy, E_H is the Hartree energy, E_{ext} is the interaction energy with the external field, and E_{xc} is the exchange-correlation energy. Both E_{ext} and E_H are already known as functionals of the density but the kinetic energy T and the exchange correlation energy E_{xc} are not known as functionals of the density. There is a good approximation for the exchange-correlation energy, the LDA, but there is no reliable approximation for the kinetic energy functional. The Hohenberg-Kohn theorem is conceptually appealing but from practical point of view it does not provide any prescription as to how to compute any physical quantities.

1.3.2 The Kohn-Sham scheme

A practical scheme for computing the ground-state energy of interacting electrons is provided by the Kohn-Sham scheme. A key concept in this scheme is the introduction of an auxiliary noninteracting system with the same ground-state density as the true interacting electron system [5]. The problem of finding a good kinetic energy functional is now circumvented by replacing it by the kinetic energy of the auxiliary noninteracting system:

$$T_0[\rho] = -\frac{1}{2}\sum_i^N \int d^3r \phi_i^*(\boldsymbol{r})\nabla^2\phi_i(\boldsymbol{r}). \tag{1.12}$$

The total energy is now written as,

$$E[\rho] = T_0[\rho] + E_H[\rho] + E_{\text{ext}}[\rho] + E_{\text{xc}}[\rho]. \tag{1.13}$$

The exchange-correlation now contains the difference between the interacting and noninteracting kinetic energy.

Pivotal to the scheme is the variational property of the total energy with respect to the ground-state density. Variation of equation (1.13) with respect to the density with a fixed number of electrons gives the Kohn-Sham equation:

$$-\frac{1}{2}\nabla^2\phi_i(\boldsymbol{r}) + V_{\mathrm{KS}}\phi_i(\boldsymbol{r}) = \epsilon_i\phi_i(\boldsymbol{r}), \tag{1.14}$$

where the Kohn-Sham potential is given by,

$$\begin{aligned} V_{\mathrm{KS}}(\boldsymbol{r}) &= \frac{\delta E_H[\rho]}{\delta\rho(\boldsymbol{r})} + \frac{\delta E_{\mathrm{ext}}[\rho]}{\delta\rho(\boldsymbol{r})} + \frac{\delta E_{\mathrm{XC}}[\rho]}{\delta\rho(\boldsymbol{r})} \\ &= V_H(\boldsymbol{r}) + V_{\mathrm{ext}}(\boldsymbol{r}) + V_{\mathrm{XC}}(\boldsymbol{r}). \end{aligned} \tag{1.15}$$

Thus, in the Kohn-Sham scheme the central quantity is the exchange-correlation energy functional. The exact functional is not known but fortunately there is a well known approximation that has been found to be very successful, namely, the Local Density Approximation, (LDA).

The exchange-correlation energy can be calculated exactly for the uniform electron gas model. In the LDA the exchange-correlation energy of the inhomogeneous system is calculated as follows:

$$E^{\mathrm{LDA}}[\rho] = \int d^3r\,\rho(\boldsymbol{r})\epsilon^{\mathrm{LDA}}\big(\rho(\boldsymbol{r})\big), \tag{1.16}$$

where $\epsilon^{\mathrm{LDA}}(\rho)$ is the exchange-correlation energy derived for the homogeneous electron gas system as a function of the density.

2 The *GW* method

2.1 Motivation

DFT within the LDA has achieved tremendous success in the field of electronic structure of materials. With the exception of strongly correlated materials (materials whose valence bands are dominated by the 3d or 4f electrons), physical properties which are intrinsically ground-state properties are generally well accounted for by the LDA. Even band structure, which is strictly speaking beyond the scope of DFT since DFT is derived from the ground-state, is in many cases reasonably well described. There are, however, well known problems which are systematic in character. One of these is the underestimation of band gaps in semiconductors and insulators as illustrated in figure 2.

The *GW* method, derived from many-body perturbation theory, can fix some of the problems in DFT. In particular, the problem of band-gap underestimation in the LDA is solved in most cases by the *GW* method as illustrated in figure 2. The theory, describing the system with the Green function, the dynamically screened Coulomb interaction and the nonlocal and energy-dependent self-energy, has proved to work successfully with a wide variety of materials, with the exception of strongly correlated materials.

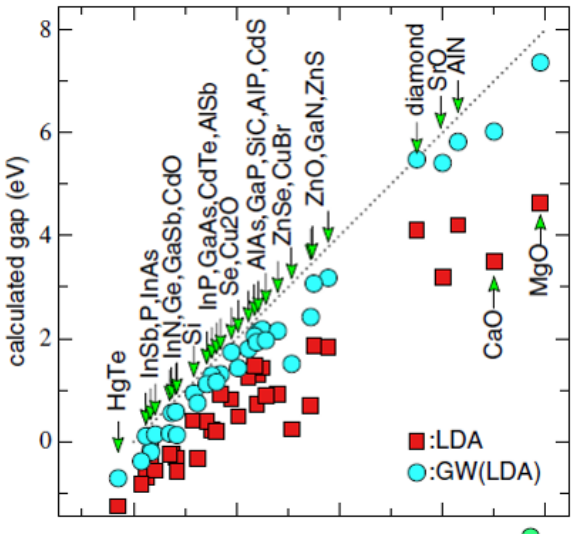

Figure 2: A comparison between calculated energy gap (LDA, square and GW, circle) and measured energy gap (dotted line), from [10]

2.2 The Green function

The Green function is useful tool for studying the electronic structure of an interacting many-particle system. It is a quantity which describes the system's response to a testing probe. The definition is given[11], by

$$\begin{aligned} G(\boldsymbol{r}t, \boldsymbol{r}'t') &= -i\Big\langle \Psi_0 \big| T[\hat{\psi}(\boldsymbol{r}t)\hat{\psi}^\dagger(\boldsymbol{r}'t')] \big| \Psi_0 \Big\rangle \\ &= \begin{cases} - & i\big\langle \Psi_0 | \hat{\psi}(\boldsymbol{r}t)\hat{\psi}^\dagger(\boldsymbol{r}'t') | \Psi_0 \big\rangle, \qquad t > t' \\ & i\big\langle \Psi_0 | \hat{\psi}^\dagger(\boldsymbol{r}'t')\hat{\psi}(\boldsymbol{r}t) | \Psi_0 \big\rangle, \qquad t < t', \end{cases} \end{aligned} \tag{2.1}$$

where Ψ_0 is the many-particle ground state and the field operator is defined in the Heisenberg picture as,

$$\hat{\psi}(\boldsymbol{r}t) = e^{i\hat{H}t}\hat{\psi}(\boldsymbol{r})e^{-i\hat{H}t}, \tag{2.2}$$

where $\hat{H}$ is the Hamiltonian of the many-particle system. The Green function is the probability amplitude of creating a particle at position $\boldsymbol{r}'$ and time t' and finding it at position $\boldsymbol{r}$ at a later time t. Or the probability amplitude of creating a hole at position $\boldsymbol{r}$ and time t and finding it at position $\boldsymbol{r}'$ at a later time t'. With the Green function, the expectation value of a single-particle operator in the ground state and the total ground-state energy can be calculated. More importantly, the one-particle excitation energies determining the band structure can be extracted from the Green function.

When the Hamiltonian is time-independent, the Green function depends only on the difference of t and t':

$$G(\boldsymbol{r}t,\boldsymbol{r}'t') = G(\boldsymbol{r},\boldsymbol{r}';\tau=t-t') = \begin{cases} -\ i\sum_n \big\langle\Psi_0|\hat{\psi}(\boldsymbol{r})|\Psi_n^{N+1}\big\rangle\big\langle\Psi_n^{N+1}|\hat{\psi}^\dagger(\boldsymbol{r}')|\Psi_0\big\rangle e^{-i(E_n^{N+1}-E_0)(t-t')}, & t>t' \\ \quad i\sum_n \big\langle\Psi_0|\hat{\psi}^\dagger(\boldsymbol{r}')|\Psi_n^{N-1}\big\rangle\big\langle\Psi_n^{N-1}|\hat{\psi}(\boldsymbol{r})|\Psi_0\big\rangle e^{i(E_n^{N-1}-E_0)(t-t')}, & t<t', \end{cases} \tag{2.3}$$

where complete sets of $N\pm1$ eigenstates of $\hat{H}$ have been inserted in between the field operators. From the Heisenberg equation of motion, the equation of motion of the Green function is given by

$$\left(i\frac{\partial}{\partial t}-h_0(\boldsymbol{r})\right)G(\boldsymbol{r}t,\boldsymbol{r}'t') + i\int d\boldsymbol{r}'' v(\boldsymbol{r}-\boldsymbol{r}'')G^{(2)}(\boldsymbol{r}t,\boldsymbol{r}'t',\boldsymbol{r}''t,\boldsymbol{r}''t^+) = \delta(t-t')\delta(\boldsymbol{r}-\boldsymbol{r}'), \tag{2.4}$$

where h_0 is the one-particle part of $\hat{H}$ and $G^{(2)}$ is the two-particle Green function

$$G^{(2)}(1,2,3,4) = (-i)^2\Big\langle\Psi_0\Big|T[\hat{\psi}(1)\hat{\psi}(3)\hat{\psi}^\dagger(4)\hat{\psi}^\dagger(2)]\Big|\Psi_0\Big\rangle. \tag{2.5}$$

We have used a notation where $1=(\boldsymbol{r}_1,t_1)$, etc. The equation of motion of the one-particle Green function is coupled to the two-particle Green function. Similarly, the equation of motion of the two-particle Green will be coupled to the three-particle Green function and so forth. To break the hierarchy, the mass operator M is introduced, requiring

$$i\int d\boldsymbol{r}'' v(\boldsymbol{r}-\boldsymbol{r}'')G^{(2)}(\boldsymbol{r}t,\boldsymbol{r}'t',\boldsymbol{r}''t,\boldsymbol{r}''t^+) = -\int d\boldsymbol{r}''dt''M(\boldsymbol{r}t,\boldsymbol{r}''t'')G(\boldsymbol{r}''t'',\boldsymbol{r}'t'). \tag{2.6}$$

When the mass operator is equal to the Hartree potential

$$M(\boldsymbol{r}t,\boldsymbol{r}'t') = V_H(\boldsymbol{r}t)\delta(\boldsymbol{r}-\boldsymbol{r}')\delta(t-t'), \tag{2.7}$$

the solution to (2.4) is defined to be the non-interacting Green function

$$\left(i\frac{\partial}{\partial t}-h(\boldsymbol{r})\right)G^0(\boldsymbol{r}t,\boldsymbol{r}'t') = \delta(t-t')\delta(\boldsymbol{r}-\boldsymbol{r}'), \tag{2.8}$$

where $h=h_0+V_H$.

The Fourier transform

$$G(\boldsymbol{r},\boldsymbol{r}';\omega) = \int_{-\infty}^{\infty} d\tau e^{i\omega\tau}G(\boldsymbol{r},\boldsymbol{r}';\tau) \tag{2.9}$$

gives the spectral representation:

$$G(\boldsymbol{r},\boldsymbol{r}';\omega) = \lim_{\delta\to0}\sum_n\left[\frac{\big\langle\Psi_0|\hat{\psi}^\dagger(\boldsymbol{r}')|\Psi_n^{N-1}\big\rangle\big\langle\Psi_n^{N-1}|\hat{\psi}(\boldsymbol{r})|\Psi_0\big\rangle}{\omega+E_n^{N-1}-E_0-i\delta} + \frac{\big\langle\Psi_0|\hat{\psi}(\boldsymbol{r})|\Psi_n^{N+1}\big\rangle\big\langle\Psi_n^{N+1}|\hat{\psi}^\dagger(\boldsymbol{r}')|\Psi_0\big\rangle}{\omega-E_n^{N+1}+E_0+i\delta}\right]. \tag{2.10}$$

The imaginary part of the Green function represents the one-particle excitation spectrum measurable in photoemission and inverse photoemission experiments. Peaks in Im $G(\omega)$ reveal quasiparticle excitations and other collective excitations in the many-particle system. The width of a peak is a measure of the life-time of the excitation. The spectral representation of the non-interacting Green function is

$$G^0(r,r';\omega) = \sum_n^{\text{occ}} \frac{\phi_n(r)\phi_n^*(r')}{\omega - \epsilon_n - i\delta} + \sum_n^{\text{unocc}} \frac{\phi_n(r)\phi_n^*(r')}{\omega - \epsilon_n + i\delta}. \tag{2.11}$$

Here, Im $G(\omega)$ comprises a series of δ-functions reflecting the infinite life-time of the excitations, since the system is noninteracting.

2.3 The screened interaction

When an electron is excited from the originally occupied location and leaves a vacancy, the remaining system can be regarded as electrons in the electric field created by the hole which carries a positive charge. The hole induces a screening charge around it so that averaged over a long period of time the interaction between the hole at $\boldsymbol{r}$ and an electron at $\boldsymbol{r'}$ is a screened Coulomb interaction, described by the screened interaction

$$W(\boldsymbol{r},\boldsymbol{r'}) = \int d^3r'' \varepsilon^{-1}(\boldsymbol{r},\boldsymbol{r''}) v(\boldsymbol{r''} - \boldsymbol{r'}), \tag{2.12}$$

where ε^{-1} is the inverse dielectric function. In general, the screened interaction depends on the frequency.

The screened interaction W plays a crucial role in determining the electronic structure of a solid. For example, the too wide occupied band width of the electron gas in the HFA is reduced back to approximately its free-electron value when screening is taken into account. It is also known that the band gaps in semiconductors and insulators are usually overestimated in the HFA and they are reduced significantly by the screened interaction.

2.4 The self energy

In density functional theory, the potential felt by each electron is approximated by the Kohn-Sham potential consisting of the external field V_{ext}, the Hartree potential V_H and the exchange-correlation potential V_{xc}, which is local and independent of the energy of the electron. However, the interaction between the electron and the surrounding background is affected by the state of the electron itself. We then expect from physical ground that the exchange-correlation potential is nonlocal and energy dependent. The nonlocal and energy-dependent potential that accounts for exchange and correlations is called the self energy $\Sigma(\boldsymbol{r},\boldsymbol{r'};E)$.

Replacing the energy-independent exchange-correlation term in DFT (1.14) with the self energy, we get the quasiparticle equation,

$$\left[-\frac{1}{2}\nabla^2 + V_H(\boldsymbol{r}) + V_{\text{ext}}(\boldsymbol{r}) \right] \Psi_i(\boldsymbol{r}) + \int d^3r' \Sigma(\boldsymbol{r},\boldsymbol{r'};E_i)\Psi_i(\boldsymbol{r'}) = E_i \Psi_i(\boldsymbol{r}). \tag{2.13}$$

The self energy is defined as the mass operator without the Hartree potential.

$$\Sigma(\boldsymbol{r}t, \boldsymbol{r'}t') = M(\boldsymbol{r}t, \boldsymbol{r'}t') - V_H(\boldsymbol{r}t)\delta(\boldsymbol{r} - \boldsymbol{r'})\delta(t - t'). \tag{2.14}$$

Similar to the analysis in 2.2, it is useful to perform a Fourier transform on the self energy,

$$\Sigma(\boldsymbol{r}, \boldsymbol{r'}; \omega) = \int_{-\infty}^{\infty} d\tau e^{i\omega\tau}\Sigma(\boldsymbol{r}, \boldsymbol{r'}; \tau), \tag{2.15}$$

where $\tau = t - t'$.

2.5 The Hedin equations

The Hedin equations, derived in 1965 [7], are a set of self-consistent equations that relates the Green function G, the screened interaction W, the vertex function Λ, the polarization function P and the self energy Σ together.

$$\Sigma(1,2) = i \int d4d5W(5,1)G(1,4)\Lambda(4,2,5), \tag{2.16}$$

$$\begin{aligned}\Lambda(1,2,3) &= \delta(1-2)\delta(1-3) \\ &+ \int d4d5d6d7 \frac{\delta\Sigma(1,2)}{\delta G(4,5)} G(4,6)G(7,5)\Lambda(6,7,3),\end{aligned} \tag{2.17}$$

$$W(1,2) = v(1-2) + \int d3d4v(1-3)P(3,4)W(4,2), \tag{2.18}$$

$$P(1,2) = -i \int d3d4G(1,3)\Lambda(3,4,2)G(4,1^+), \tag{2.19}$$

$$G(1,2) = G^0(1,2) + \int d3d4G^0(1,3)\Sigma(3,4)G(4,2), \tag{2.20}$$

where the number 1 stands for (r_1, t_1), etc.

With the Hedin equations, the electronic structure of a many-electron system can be investigated in an ab initio way.

2.6 The GW approximation

To obtain the GWA, the Hedin equations are solved iteratively, starting with setting the self energy to be zero. The first iteration gives,

$$G = G^0, \tag{2.21}$$

$$\Lambda(1,2,3) = \delta(1-2)\delta(1-3), \tag{2.22}$$

$$P^0(1,2) = -iG^0(1,2)G^0(2,1^+), \tag{2.23}$$

$$W^0(1,2) = v(1-2) + \int d3d4v(1-3)P^0(3,4)W^0(4,2), \tag{2.24}$$

$$\Sigma(1,2) = iG^0(1,2)W^0(2,1), \tag{2.25}$$

3 Calculating the GW self energy of the uniform electron gas

The self energy $\Sigma(\boldsymbol{r}, \boldsymbol{r'}; \omega)$ in the GW approximation is given by,

$$\Sigma(\boldsymbol{r}, \boldsymbol{r'}; \omega) = i \int \frac{d\omega'}{2\pi} G^0(\boldsymbol{r}, \boldsymbol{r'}; \omega + \omega') W^0(\boldsymbol{r}, \boldsymbol{r'}; \omega'). \tag{3.1}$$

For uniform electron gas model, the system is isotropic, so the spatial dependence of observables is determined by the magnitude of the difference of $\boldsymbol{r}$ and $\boldsymbol{r'}$. Therefore, (3.1) simplifies to

$$\Sigma(R; \omega) = i \int \frac{d\omega'}{2\pi} G^0(R; \omega + \omega') W^0(R; \omega'), \tag{3.2}$$

where $R = |\boldsymbol{r} - \boldsymbol{r'}|$.

In order to obtain the self-energy Σ, we need to compute the screened interaction W^0. We must therefore first investigate and compute the polarization function P^0 since it determines W^0.

3.1 Polarization function

According to equation (2.23), the polarization function is constructed with the non-interacting Green function (2.11),

$$P^0(1, 2; \omega) = -i \int \frac{d\omega'}{2\pi} G^0(1, 2; \omega + \omega') G^0(2, 1; \omega'). \tag{3.3}$$

Performing a Fourier transform to the wave vector space,

$$P^0(q, \omega) = 2 \int \frac{d^3k}{(2\pi)^3} \left[\frac{1}{\omega + \omega_{\boldsymbol{k}} - \omega_{\boldsymbol{k}+\boldsymbol{q}} + i\eta} - \frac{1}{\omega - \omega_{\boldsymbol{k}} + \omega_{\boldsymbol{k}+\boldsymbol{q}} - i\eta} \right] \times \theta(k_F - k)\theta(|\boldsymbol{k} + \boldsymbol{q}| - k_F), \tag{3.4}$$

where θ is the Heaviside step function standing for,

$$\begin{aligned} k < k_F, \quad & \text{occupied states} \\ |\boldsymbol{k} + \boldsymbol{q}| > k_F, \quad & \text{unoccupied states.} \end{aligned} \tag{3.5}$$

The calculation of P^0 (eq. (3.4)) can be done analytically[11], but the form of P^0 contains a singularity, which poses numerical difficulties in calculating the self energy. Therefore, P^0 was calculated using numerical methods.

3.1.1 Imaginary part of P^0

The imaginary part of P^0 is given by,

$$\begin{aligned}\text{Im } P^0(q,\omega) &= 2\int \frac{d^3k}{(2\pi)^3}\Big[-\pi\delta\big(\omega+\omega_{\boldsymbol{k}}-\omega_{\boldsymbol{k}+\boldsymbol{q}}\big)-\pi\delta\big(\omega-\omega_{\boldsymbol{k}}+\omega_{\boldsymbol{k}+\boldsymbol{q}}\big)\Big] \\ &\qquad\qquad \times\theta(k_F-k)\theta(|\boldsymbol{k}+\boldsymbol{q}|-k_F) \\ &= 2\int \frac{d^3k}{(2\pi)^3}\Big[-\pi\delta\big(\omega-\frac{1}{2}q^2-kqy\big)-\pi\delta\big(\omega+\frac{1}{2}q^2+kqy\big)\Big] \\ &\qquad\qquad \times\theta(k_F-k)\theta(|\boldsymbol{k}+\boldsymbol{q}|-k_F),\end{aligned} \tag{3.6}$$

where $y=\hat{\boldsymbol{q}}\cdot\hat{\boldsymbol{k}}$. The factor of 2 accounts for the two spin channels.

The polarization function has the symmetry $P(q,\omega)=P(q,-\omega)$. The numerical integration is done with the positive frequency part of equation (3.6). The delta function represents the energy conservation relation,

$$\begin{aligned}\omega &= \omega_{\boldsymbol{k}+\boldsymbol{q}}-\omega_{\boldsymbol{k}} \\ &= \frac{1}{2}q^2+kqy,\end{aligned} \tag{3.7}$$

which can be approximated by a Gaussian function,

$$\delta\big(\omega-\frac{1}{2}q^2-kqy\big)\to\frac{1}{\sqrt{\pi}\sigma}e^{-(\omega-\frac{1}{2}q^2-kqy)^2/\sigma^2}=\sqrt{\frac{\alpha}{\pi}}e^{-\alpha(\omega-\frac{1}{2}q^2-kqy)^2}, \tag{3.8}$$

where $\sigma=1/\sqrt{\alpha}$ is a parameter determining the width of the Gaussian.

The Heaviside step function in equation (3.6) is included in the integrating interval of k. (3.6) simplifies to,

$$\text{Im } P^0(q,\omega)=\frac{2}{(2\pi)^2}\int_{|\boldsymbol{k}+\boldsymbol{q}|>k_F}^{k_F}dkk^2\int_{-1}^{1}dy\sqrt{\alpha\pi}\Big[e^{-\alpha(\omega-\frac{1}{2}q^2-kqy)^2}\Big]. \tag{3.9}$$

The integral of y in (3.9) can be expressed with the error function,

$$\begin{aligned}&\int_{-1}^{1}dy\sqrt{\alpha\pi}e^{-\alpha(\omega-\frac{1}{2}q^2-kqy)^2}=\frac{1}{kq}\int_{-\omega+\frac{1}{2}q^2-kq}^{-\omega+\frac{1}{2}q^2+kq}dx\sqrt{\alpha\pi}e^{-\alpha x^2} \\ &=\frac{\pi}{2kq}\Big[\text{Erf}[\sqrt{\alpha}(-\omega+\frac{1}{2}q^2+kq)]-\text{Erf}[\sqrt{\alpha}(-\omega+\frac{1}{2}q^2-kq)]\Big],\end{aligned} \tag{3.10}$$

where the error function is defined as,

$$\text{Erf}(x)=\frac{2}{\sqrt{\pi}}\int_0^x\exp\left(-t^2\right)dt. \tag{3.11}$$

For the integral of k in (3.9), the integrating interval of k, equivalent to $k<k_F, |\boldsymbol{k}+\boldsymbol{q}|>k_F$, varies with q. In the following analysis, k_F is set to be unity.

For large q ($q > 2$), the relation between $\boldsymbol{k}$, $\boldsymbol{q}$ and the Fermi sphere is illustrated in figure 3. Eq. (3.5) requires that the ending point of $\boldsymbol{k}+\boldsymbol{q}$ is outside the first Fermi sphere, and $\boldsymbol{k}$ is inside the second Fermi sphere. Eq. (3.7) requires that the frequency ω falls in an interval such that $\boldsymbol{k}+\boldsymbol{q}$ and $\boldsymbol{k}$ end at the same point. The minimum of k is taken when $\boldsymbol{k}$ is parallel to $\boldsymbol{q}$.

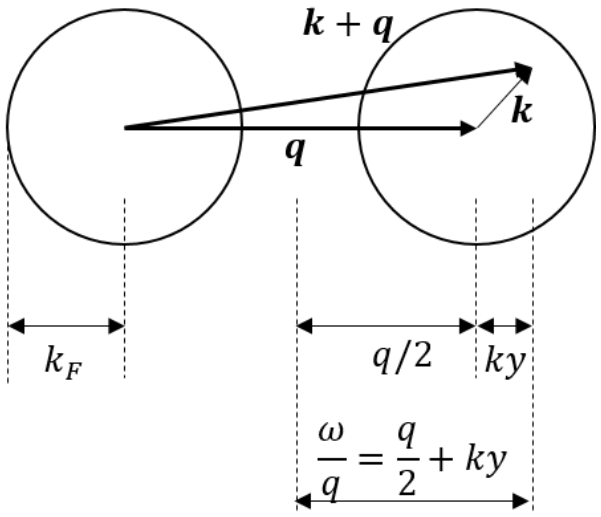

Figure 3: Illustration of the integration region for (3.9) when $q > 2k_F$

.

Then the restriction conditions of k and ω are,

$$\begin{aligned} q^2/2 - q \leq &\omega \leq q^2/2 + q \\ \omega/q - q/2 \leq &k \leq 1. \end{aligned} \tag{3.12}$$

Equation (3.9) becomes,

$$\begin{aligned} \text{Im } P^0(q,\omega) = \frac{k_F}{4\pi q}\int_{\omega/q-q/2}^{1} dk \\ \times k\left[\text{Erf}[\sqrt{\alpha}(-\omega+\frac{1}{2}q^2+kq)] - \text{Erf}[\sqrt{\alpha}(-\omega+\frac{1}{2}q^2-kq)]\right]. \end{aligned} \tag{3.13}$$

For small q ($q < 2$), when $q - q^2/2 \leq \omega \leq q^2/2 + q$ (as shown in figure 4(a)), the analysis is similar to the case of $q > 2$. The imaginary part of the polarization function has the form of equation (3.13).

However, when $\omega \leq q - q^2/2$ (as shown in figure 4(b)), the minimum of k is taken when $\boldsymbol{k}$ ends on the surface of the first Fermi sphere,

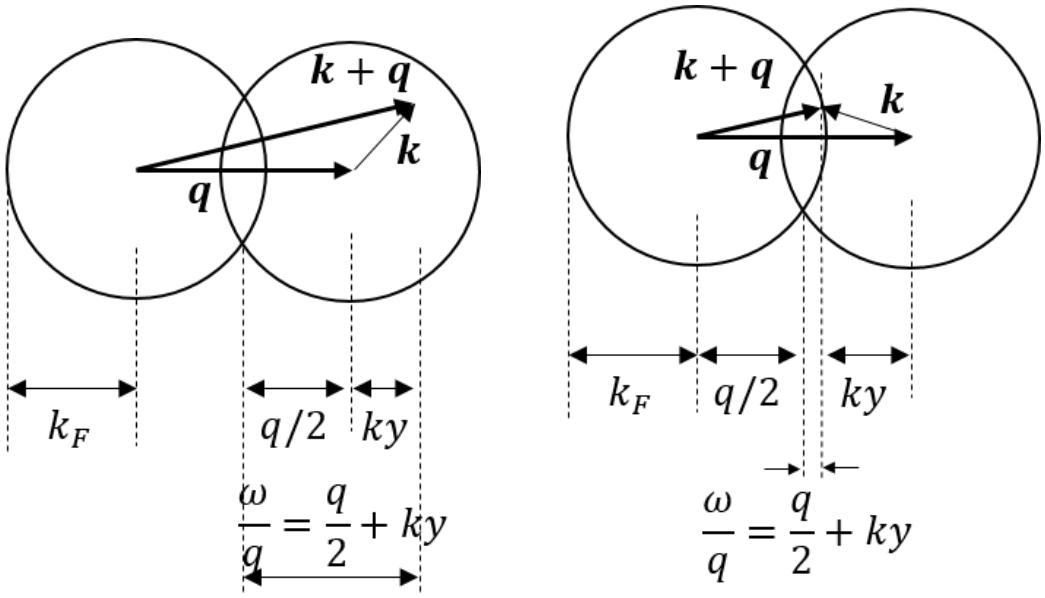

(a) $q - q^2/2 \leq \omega \leq q + q^2/2$ (b) $\omega \leq q - q^2/2$

Figure 4: Illustration of the integration region for (3.9) when $q < 2k_F$

$$k_{\min}^2 = 1 - (q/2 + \omega/q)^2 + (q/2 - \omega/q)^2 = 1 - 2\omega. \tag{3.14}$$

In this case, equation (3.9) becomes,

$$\begin{aligned} \text{Im } P^0(q,\omega) = \frac{k_F}{4\pi q} \int_{(1-2\omega)^{1/2}}^{1} dk \\ \times k\left[\text{Erf}[\sqrt{\alpha}(-\omega + \frac{1}{2}q^2 + kq)] - \text{Erf}[\sqrt{\alpha}(-\omega + \frac{1}{2}q^2 - kq)]\right]. \end{aligned} \tag{3.15}$$

The result of the numerical calculation is shown in figure 5. For large q (the case of fig. 3), the dependence of $\text{Im}P^0$ on the frequency is quadratic. The maximum value is q^{-1}. For small q, the $\text{Im}P^0 - \omega$ plot can be divided into two parts, a quadratic part (corresponding to fig. 4(a)) and a linear part (corresponding to fig. 4(b)). The maximum value is $2 - q$. The numerical result is consistent with the analytical result in [11].

3.1.2 Real part

The real part of P^0 can be calculated from the Hilbert transform,

$$\begin{aligned} \text{Re } P^0(\omega) &= -\frac{1}{\pi}\int_{-\infty}^{\infty} d\omega' \frac{\text{Im } P^0(\omega')\text{sgn}(\omega')}{\omega - \omega'} \\ &= -\frac{1}{\pi}\int_{-\infty}^{\infty} d\omega' F_H(\omega'). \end{aligned} \tag{3.16}$$

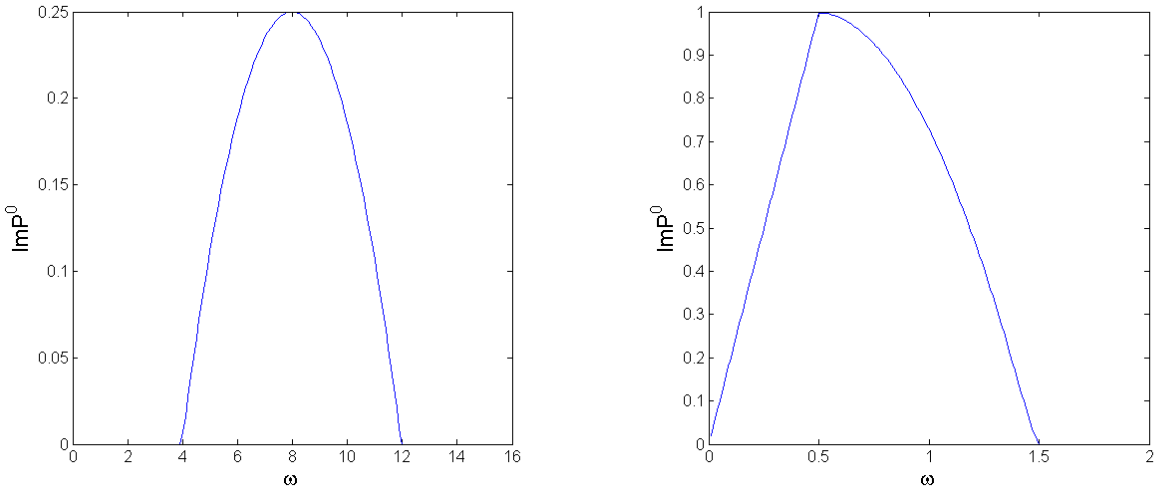

(a) $q = 4$ (b) $q = 1$

Figure 5: Imaginary part of the polarization function, multiplied by a factor of 4π. The calculation was done with the parameter $\alpha = 200$.

The integrand $F_H(\omega')$ has a singularity at $\omega' = \omega$, as shown in figure 6. The integral can be done, in principle, by the Cauchy principal value method. However, the method is

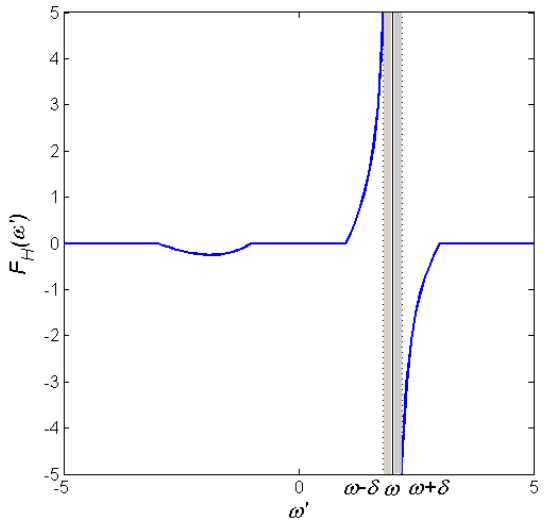

Figure 6: Stretch of a function having the same structure as the integrating function in (3.16). For an infinitesimal δ, the sum of the integral of the shadowed zones is finite, so that the integral converges to the principal value.

not convenient. When the numerical integration is repeated many times, numerical errors

will accumulate due to the limited mesh size. It is desirable to remove the singularity automatically. With the even property of $P^0(\omega)$, (3.16) can be written as,

$$\begin{aligned}
-\pi \text{Re } P^0(\omega) &= \int_{-\infty}^{0} d\omega'' \frac{\text{Im } P^0(\omega-\omega'')}{\omega''} + \int_0^{\infty} d\omega'' \frac{\text{Im } P^0(\omega-\omega'')\text{sgn}(\omega-\omega'')}{\omega''} \\
&= -\int_0^{\infty} d\omega'' \frac{\text{Im } P^0(\omega+\omega'')}{\omega''} + \int_0^{\infty} d\omega'' \frac{\text{Im } P^0(\omega-\omega'')\text{sgn}(\omega-\omega'')}{\omega''} \\
&= \int_0^{\infty} d\omega'' \frac{\text{Im } P^0(\omega-\omega'')\text{sgn}(\omega-\omega'') - \text{Im } P^0(\omega+\omega'')}{\omega''} \\
&= \int_0^{\infty} d\omega'' F_H^*(\omega''),
\end{aligned} \tag{3.17}$$

where the function $F_H^*(\omega'')$ has no singularities, as shown in figure 7. When $\omega'' \to 0$,

$$\begin{aligned}
F_H^*(0) &= \lim_{\omega''\to 0} \frac{\text{Im } P^0(\omega-\omega'') - \text{Im } P^0(\omega+\omega'')}{\omega''} \\
&= -2\frac{d}{d\omega''}\text{Im } P^0\big|_{\omega''=\omega}.
\end{aligned} \tag{3.18}$$

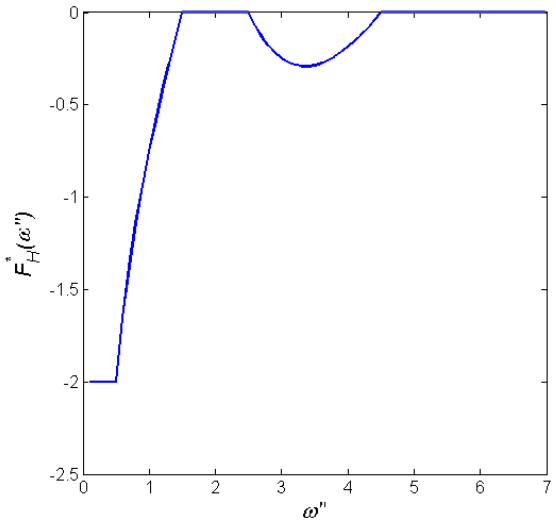

Figure 7: The change from $F_H(\omega')$ to $F_H^*(\omega'')$ removes the singularity spontaneously.

3.2 Screened interaction

To simplify writing we set $W = W^0$. The screened interaction in real space $W(R;\omega)$ is needed to calculate the self energy according to (3.1). It can be acquired by the Fourier transform from momentum space.

$$\begin{aligned} W(R,\omega) &= \int \frac{d^3q}{(2\pi)^3} e^{i\boldsymbol{q}\cdot\boldsymbol{R}} W(q,\omega) \\ &= \frac{1}{2\pi^2}\int_0^\infty dq \frac{q\sin qR}{R} W(q,\omega), \end{aligned} \tag{3.19}$$

where the screened interaction in the momentum space is given by,

$$W(q,\omega) = \frac{v(q)}{1-v(q)P^0(q,\omega)} = \frac{4\pi}{q^2 - 4\pi P^0(q,\omega)}. \tag{3.20}$$

The polarization function, as well as the screened interaction, is complex, and the real part and the imaginary part carry different physical meanings. Therefore, the two parts need to be discussed separately.

$$\begin{aligned} \text{Re } W(q,\omega) &= \frac{q^2/4\pi - \text{Re } P^0(q,\omega)}{\big(q^2/4\pi - \text{Re}P^0(q,\omega)\big)^2 + \big(\text{Im } P^0(q,\omega)\big)^2}, \\ \text{Im } W(q,\omega) &= \frac{\text{Im } P^0(q,\omega)}{\big(q^2/4\pi - \text{Re } P^0(q,\omega)\big)^2 + \big(\text{Im } P^0(q,\omega)\big)^2}. \end{aligned} \tag{3.21}$$

The integral in equation (3.19) has a term $\sin qR$, which oscillates rapidly as a function of q when R is large. Therefore, the integral is done with Filon's integration formula [12].

$$\begin{aligned} I_{\text{filon}} &= \int_\Delta^\Lambda W(q)\sin(Rq)dq \\ &= h\Big\{\alpha(Rh)\big[W(\Delta)\cos(R\Delta) - W(\Lambda)\cos(R\Lambda)\big] + \beta(Rh)S_e + \gamma(Rh)S_o\Big\} \\ \alpha(\theta) &= \frac{1}{\theta} + \frac{\sin 2\theta}{2\theta^2} - \frac{2\sin^2\theta}{\theta^3} \\ \beta(\theta) &= \frac{1}{\theta^2} + \frac{\cos^2\theta}{\theta^2} - \frac{\sin 2\theta}{\theta^3} \\ \gamma(\theta) &= \frac{4\sin\theta}{\theta^3} - \frac{4\cos\theta}{\theta^2} \\ S_e &= W(\Delta)\sin(R\Delta) - W(\Lambda)\sin(R\Lambda) + 2\sum_{i=1}^{N} W(\Delta+2ih)\sin(R\Delta+2iRh) \\ S_o &= \sum_{i=1}^{N} W[\Delta+(2i-1)h]\sin[R\Delta+(2i-1)Rh], \end{aligned} \tag{3.22}$$

where Δ and Λ are the lower limit and the upper limit, respectively. h is the mesh size. With the number of meshes to be $2N$, the parameters fulfill that,

$$h = \frac{\Lambda - \Delta}{2N}. \tag{3.23}$$

The upper limit can be determined from the condition,

$$W(q > \Lambda, \omega) = 0. \tag{3.24}$$

$W(q, \omega)$ diverges as $q \to 0$, which means the lower limit can not be set to zero. To get the complete screened function, a part I_c needs to be added and treated analytically,

$$\begin{aligned} W(R, \omega) &= I_{\text{filon}} + I_c \\ &= I_{\text{filon}} + \frac{1}{2\pi^2} \int_0^{\Delta} dq \frac{q \sin qR}{R} W(q, \omega). \end{aligned} \tag{3.25}$$

For Δ small enough, $W(q) \sim q^{-2}$, so the compensation part can be calculated as,

$$\begin{aligned} I_c &= \frac{1}{2\pi^2} \int_0^{\Delta} dq \frac{q \sin qR}{R} \frac{W(\Delta)\Delta^2}{q^2} \\ &= \frac{W(\Delta)\Delta^2}{2\pi^2 R} \int_0^{R\Delta} \frac{\sin x}{x} dx \\ &\approx \frac{W(\Delta)\Delta^2}{2\pi^2 R} \int_0^{R\Delta} \frac{x - x^3/6}{x} dx \\ &= \frac{W(\Delta)\Delta^2}{2\pi^2 R} \big[R\Delta - (R\Delta)^3/18\big]. \end{aligned} \tag{3.26}$$

3.2.1 A benchmark test at large frequency

When the frequency of the perturbation is large enough, the system cannot react immediatel so that the polarization function tends to zero. Therefore, the screening effect is not present, and the screened interaction goes over to the bare Coulomb interaction,

$$\begin{aligned} W(q, \omega \gg k_F^2) &= v(q) = \frac{4\pi}{q^2}, \\ W(R, \omega \gg k_F^2) &= \frac{2}{\pi} \int_0^{\infty} dq \frac{\sin qR}{qR} = \frac{1}{R}. \end{aligned} \tag{3.27}$$

The result is shown in figure 8

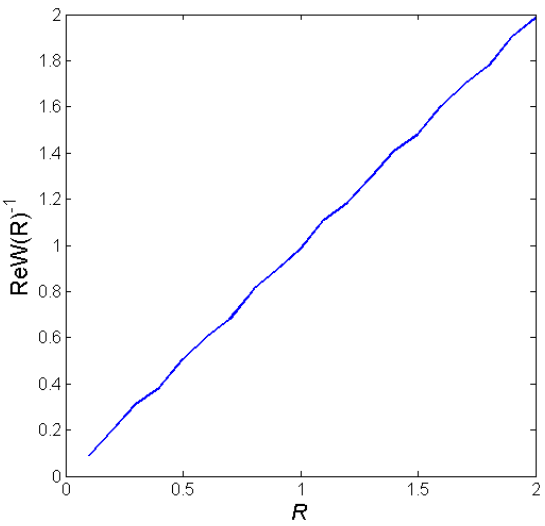

Figure 8: Plot of $1/\text{Re}\ W(R)$ vs. R, computed with the frequency $\omega = 10k_F^2$. The linear behavior shows that at high frequency, the screened interaction goes over to the bare Coulomb interaction.

3.3 Self energy

From (3.2), the self energy can be calculated, and the detailed derivation is in the appendix. For the real part, we have

$$\begin{aligned}\text{Re}\ \Sigma(R,\omega) = &-\sum_k^{\text{occ}} \psi_k(\boldsymbol{r})\psi_k^*(\boldsymbol{r'})\text{Re}\ W(R,\omega-\epsilon_k) \\ &+\sum_k \psi_k(\boldsymbol{r})\psi_k^*(\boldsymbol{r'})\text{P}\int_0^\infty d\omega' \frac{D(R,\omega')}{\omega-\epsilon_k-\omega'},\end{aligned} \tag{3.28}$$

where

$$D(R,\omega') = -\frac{1}{\pi}\text{Im}\ W(R,\omega')\text{sgn}(\omega'). \tag{3.29}$$

The self energy in the GWA can be naturally decomposed into the sum of two parts: screened exchange part (SEX) and Coulomb-hole part (COH).

3.3.1 Screened exchange part

The first term in the right hand side of (3.28) has the same form as the bare exchange potential,

$$\Sigma_{\text{X}}(R) = -v(R)\sum_k^{\text{occ}} \psi_k(\boldsymbol{r})\psi_k^*(\boldsymbol{r'}), \tag{3.30}$$

except that the dynamical screened potential W is used instead of the bare Coulomb potential v. Therefore, this term represents the screened exchange:

$$\begin{aligned}\text{Re } \Sigma_{\text{SEX}}(R,\omega) &= -\sum_{k}^{\text{occ}} \psi_k(\boldsymbol{r})\psi_k^*(\boldsymbol{r'})\text{Re } W(R,\omega-\epsilon_k) \\ &= -\frac{1}{2\pi^2}\int_0^{k_F} dk \frac{k\sin kR}{R}\text{Re } W(R,\omega-\epsilon_k),\end{aligned} \tag{3.31}$$

where for the homogeneous electron gas the last line has been obtained by replacing the wave functions by plane waves.

The validity of the result can be verified by comparing with the static approximation, which corresponds to $\omega - \epsilon_k \to 0$ in (3.31). Then $W(R, \omega - \epsilon_k)$ can be approximated with $W(R, \omega = 0)$,

$$\text{Re } \Sigma_{\text{SEX}}^{\text{static}}(R) = -\frac{\text{Re } W(R,0)}{2\pi^2}\int_0^{k_F} dk \frac{k\sin kR}{R} \tag{3.32}$$

where the integral in the right hand side can be calculated analytically

$$\begin{aligned} I &= \int_0^{k_F} dk \frac{k\sin kR}{R} \\ &= \frac{1}{R^2}\big[\frac{\sin(k_F R)}{R} - k_F\cos(k_F R)\big].\end{aligned} \tag{3.33}$$

When only the states close to the Fermi level ($\omega \approx k_F^2/2$) are of interest, the result of (3.31) should go over to the static approximation (3.32), as shown in figure 9. On the other hand, in the low frequency limit, the screened interaction $W(R,\omega)$ can be approximated by the Yukawa potential,

$$V^{\text{Yukawa}} = \frac{e^{-k_F R}}{R}. \tag{3.34}$$

In such limit, the static approximation (3.32) becomes,

$$\Sigma_{\text{SEX}}^{\text{Yukawa}} = -\frac{1}{2\pi^2}\frac{e^{-k_F R}}{R^3}\big[\frac{\sin(k_F R)}{R} - k_F\cos(k_F R)\big]. \tag{3.35}$$

This result is also compared in figure 9. The Wigner-Seitz radius R_{WS} is used as the unit of distance in the figures below, defined by,

$$R_{\text{WS}} = (\frac{3}{4\pi n})^{1/3} = \frac{1.92}{k_F}, \tag{3.36}$$

where n is the electron density. The energy is in the unit of the Fermi energy. In such scale, the real space behavior of the self-energy is generic.

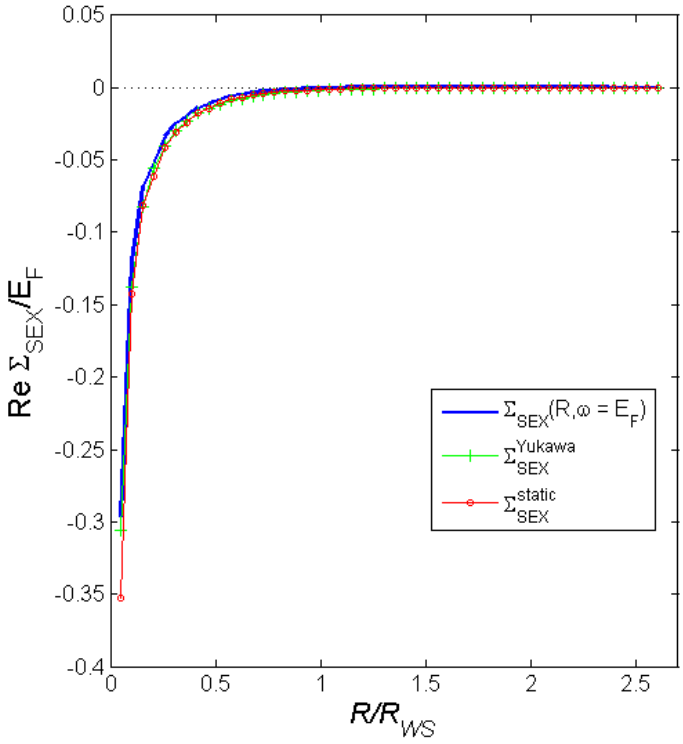

Figure 9: The numerical result of (3.31) at $\omega = \frac{1}{2}k_F^2$ is consistent with the static approximation, which supports the validity of the calculations. Calculated with $k_F = 1$, corresponding to $R_{\rm WS} = 1.92$.

3.3.2 Coulomb hole part

The physical meaning of the second term in the right hand side of (3.28) can be understood under the static COHSEX approximation in which $\omega - \epsilon_k \to 0$, which gives,

$$\begin{aligned} \text{Re } \Sigma_{\rm COH}^{\rm static}(R) &= \frac{1}{2}\delta(R)\big[W(R,\omega=0) - v(R)\big] \\ &= \frac{1}{2}\delta(R)W_{\rm c}(R,0). \end{aligned} \tag{3.37}$$

The result has the form of Coulomb interaction, thus can be interpreted as the interaction between an electron and the potential created by its screening hole. The factor of $1/2$ represents an adiabatic process that the interaction increases from zero to $W_{\rm c}(R,0)$.

The numerical calculation of the Coulomb hole term goes as follows:

$$\begin{aligned}\text{Re } \Sigma_{\text{COH}}(R,\omega) &= \sum_k \psi_k(\boldsymbol{r})\psi_k^*(\boldsymbol{r'})\text{P}\int_0^\infty d\omega' \frac{D(R,\omega')}{\omega-\epsilon_k-\omega'} \\ &= \frac{1}{2\pi^2}\int_0^\infty dk \frac{k\sin kR}{R}\text{P}\int_0^\infty d\omega' \frac{D(R,\omega')}{\omega-\epsilon_k-\omega'} \\ &= \frac{1}{2\pi^2}\int_0^\infty dk \frac{k\sin kR}{R} F(R,\omega-\epsilon_k),\end{aligned} \tag{3.38}$$

where

$$\begin{aligned}D(R,\omega') &= -\frac{1}{\pi}\text{Im } W(R,\omega')\text{sgn}(\omega') \\ F(R,\omega-\epsilon_k) &\equiv \text{P}\int_0^\infty d\omega' \frac{D(R,\omega')}{\omega-\epsilon_k-\omega'}.\end{aligned} \tag{3.39}$$

The calculation of Re Σ_{COH} (3.38) contains two parts: a Hilbert transform (3.39) and an integral over k of a rapidly-oscillating function. The same methods employed in Sections 3.1.2 and 3.2 can be used here.

A plot of the F function at some characteristic frequencies is shown in figure 10. The magnitude of $F(R,\omega)$ decreases with R, due to the decrease of Im W with R. $D(\omega')$ is negative until ω' is large enough, then it remains zero. Therefore, F is mainly negative at high frequency and positive at low frequency.

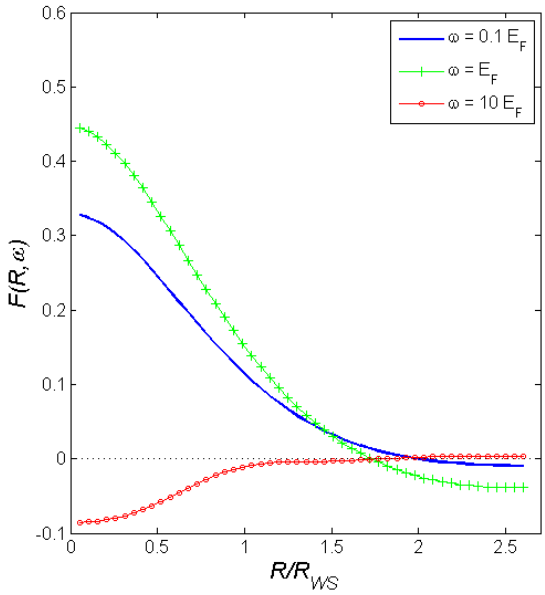

Figure 10: A plot of the F function in (3.39) at different frequencies, calculated with $k_F = 1$ corresponding to $R_{\text{WS}} = 1.92$

4 Results

In the following, the results are presented for the case of $k_F = 1$ corresponding to $R_{\mathrm{WS}} = 1.92$. The real space behavior of the screened-exchange term is shown in figure 11(a). The screened-exchange self-energy shows a weak dependence on frequency. At certain frequencies, part of Re Σ_{SEX} becomes positive. At the large frequency limit, as expected the screened-exchange term approaches the bare exchange potential, given by

$$\begin{aligned} \Sigma_{\mathrm{X}} &= -\frac{v(R)}{2\pi^2}\int_0^{k_F} dk \frac{k \sin kR}{R} \\ &= -\frac{1}{2\pi^2 R^4}\left[\sin\left(k_F R\right) - k_F R \cos\left(k_F R\right)\right]. \end{aligned} \tag{4.1}$$

The screened-exchange self-energy is for the most part localized within the Wigner-Seitz radius, which means the localized static approximation works well. However, the change of sign at intermediate frequencies ($\approx 2E_F$) is not captured by the static approximation.

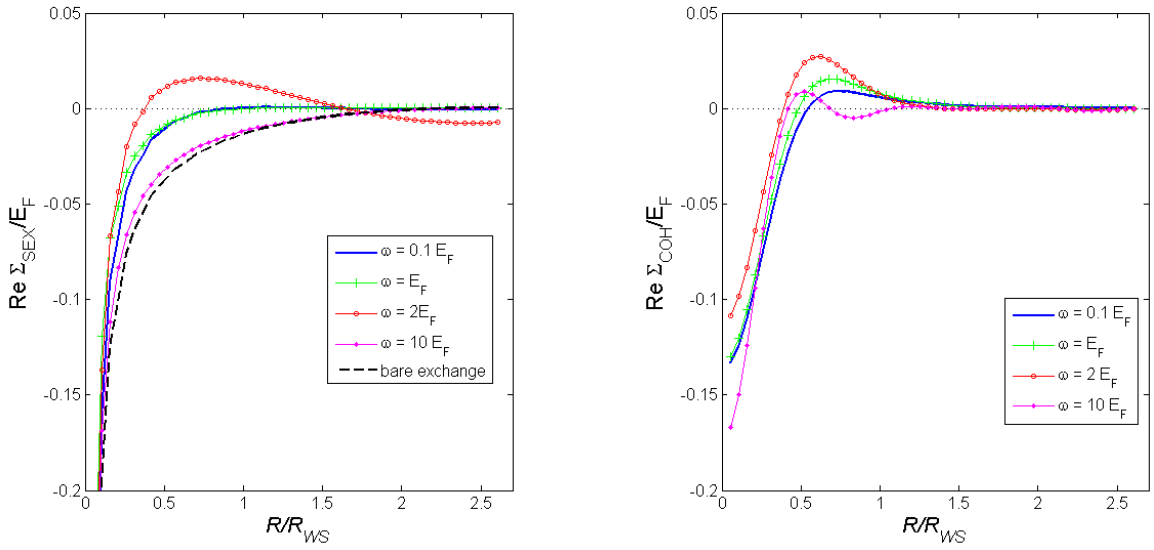

(a) Screened-exchange term

(b) Coulomb-hole term

Figure 11: (a) The real part of the screened-exchange term. At high frequency, Re Σ_{SEX} approaches the bare exchange potential, as it should. (b) The real part of the Coulomb-hole term. Both calculated with $k_F = 1$ corresponding to $R_{\mathrm{WS}} = 1.92$.

The real space behavior of the Coulomb-hole term is shown in figure 11(b). Contrary to the static COHSEX approximation, Re Σ_{COH} does not resemble a delta function. In fact, it is more broadened compared with the screened-exchange term. Indeed, calculations on real materials based on the static COHSEX approximation are not generally in good agreement with the full GW calculations. The present study reveals that the discrepancy most likely originates from the approximation on the Coulomb-hole term. As the frequency decreases and is comparable to the Fermi energy, the degree of localization decreases. As the frequency increases the Coulomb-hole term displays more pronounced oscillations in space. This can be understood by considering the high-frequency limit as the short-time limit within which the creation of a hole or the addition of a particle takes place that causes a sudden perturbation to the system resulting in an oscillatory behavior. It may also explain why the self-energy is more localized at high frequency since the screening charge density does not have sufficient time to relax and rearrange itself into a more optimal distribution. In comparison to the screened-exchange term, the Coulomb-hole term shows a stronger dependence on the frequency but it is mainly localized within the Wigner-Seitz radius.

All the discussions above are based on setting $k_F = 1$, which refers to a fixed electron density. However, the density of the electron gas affects the degree of screening, thus the self-energy. To investigate the effects of the density, calculations under different k_F values were conducted. For real materials, the density of electrons typically corresponds to the Wigner-Seitz radius between 3-5, therefore R_{WS} was set to be 2, 4 and 6. For example, the average valence electron density in sodium and transition metals approximately correspond to $R_{\mathrm{WS}} \approx 4$ and $R_{\mathrm{WS}} \approx 2$, respectively. The results of Σ_{SEX} and Σ_{COH} at the Fermi energy are shown in figure 12.

It is very interesting to observe that the screened-exchange term at the Fermi energy is essentially negative for all distance and can be very well approximated by an exchange potential with a Yukawa interaction characterized in range by the Fermi momentum. This opens up a possibility of using the Yukawa interaction for the screened exchange term for real materials but with a varying Fermi momentum depending on the local density. The Coulomb-hole term, on the other hand, shows a more complex behavior. The Coulomb-hole term in the static COHSEX approximation sometimes used in GW calculations does not appear to be a good approximation since the true Coulomb-hole potential does not resemble a delta function. At low density, the Coulomb-hole term tends to be repulsive between $R = 0.25 - 0.50\ R_{\mathrm{WS}}$, reminiscence of the physics of electron localization as correlation becomes stronger in the low-density limit. Electrons tend to repel each other causing localization as in the Wigner lattice.

The SEX term is more localized than the COH term, since Σ_{SEX} tends to zero rapidly.

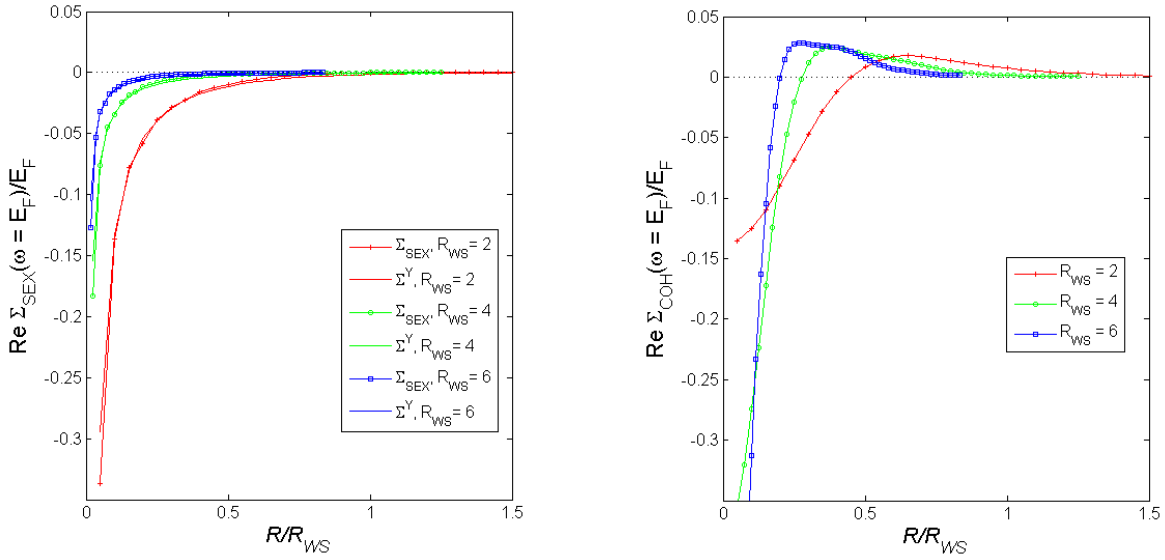

(a) Screened-exchange term

(b) Coulomb-hole term

Figure 12: The frequency is fixed to be the Fermi energy. Σ^{Y} refers to the SEX term calculated with the screening interaction equal to the Yukawa potential. Calculated with $R_{\mathrm{WS}} = 2$, 4 and 6.

The behavior of Σ_{SEX} and Σ_{COH} at different frequencies for $R_{\mathrm{WS}} = 2$ and 4 is shown in figure 13 and 14. The degree of localization increases as the density decreases. At the same electron density, the Coulomb-hole term turns positive within a shorter distance with higher frequency. Σ_{COH} of lower density shows relatively stronger repulsive behavior.

At $R \approx 0.25\ R_{\mathrm{WS}}$, the screened-exchange term of lower density is close to zero, while for the high density case, Σ_{SEX} is still remarkably negative, owing to the stronger exchange effect of the higher density. It is noteworthy that at high density the screened exchange term is dominant for small distance whereas at low density the Coulomb hole term dominates almost completely.

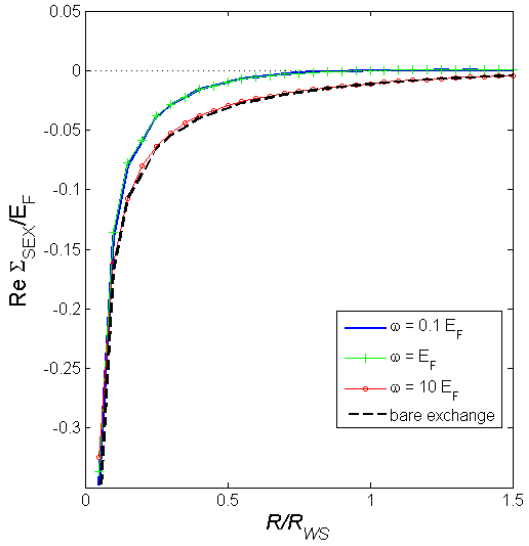

(a) $R_{\mathrm{WS}} = 2$

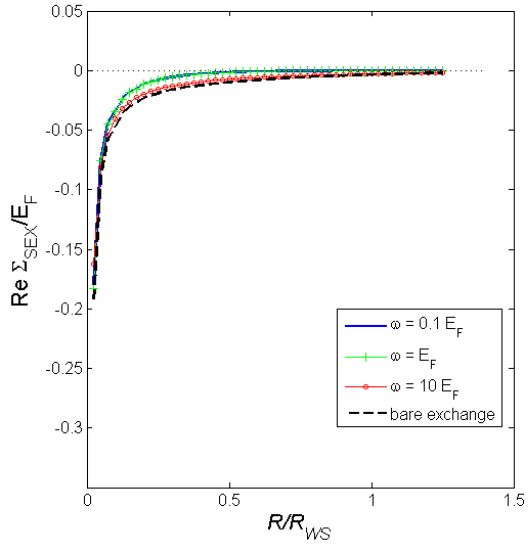

(b) $R_{\mathrm{WS}} = 4$

Figure 13: The frequency dependence of SEX term with $R_{\mathrm{WS}} = 2$ and 4.

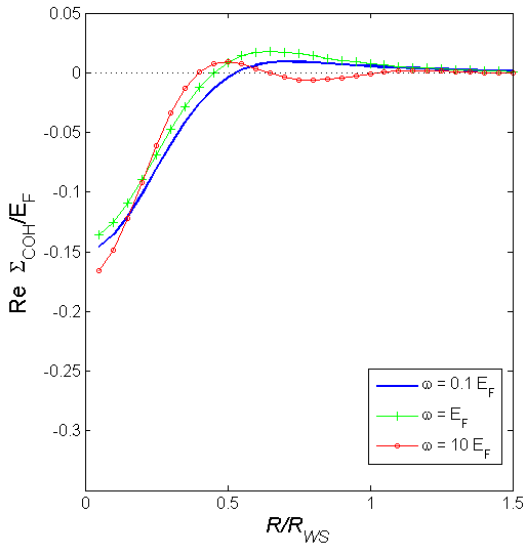

(a) $R_{\mathrm{WS}} = 2$

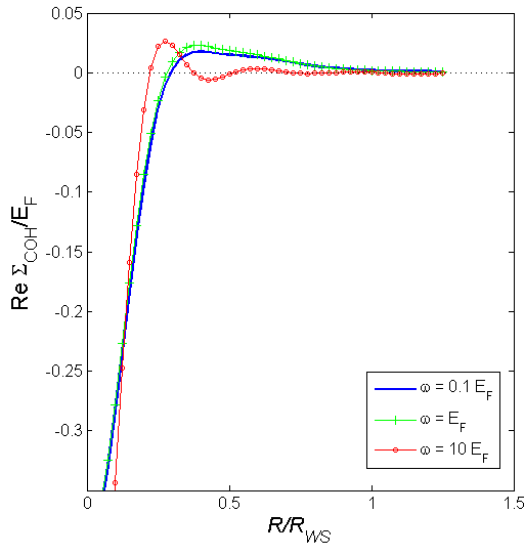

(b) $R_{\mathrm{WS}} = 4$

Figure 14: The frequency dependence of COH term with $R_{\mathrm{WS}} = 2$ and 4.

The total self-energy is shown in figure 15. It shows a dependence on the frequency, which is largely brought about by the Coulomb-hole part. The results can be compared with Hedin's calculation for $\Sigma(R, \omega = E_F)$ [13]. The self-energy increases with R and reaches a peak at R_{peak}. Then Σ decreases and tends to zero from R_{zero}. The peak is

positive except for the high density high frequency case. The positive part is mainly caused by the repulsive correlation interaction from the Coulomb term, which is essentially small for the high density case. The stronger exchange effect of the high density case contributes to the negative SEX term. These two effects lead to the negative peak. R_{peak} and R_{zero} are smaller for the low density case, indicating a higher degree of localization, which is consistent with Hedin's analysis.

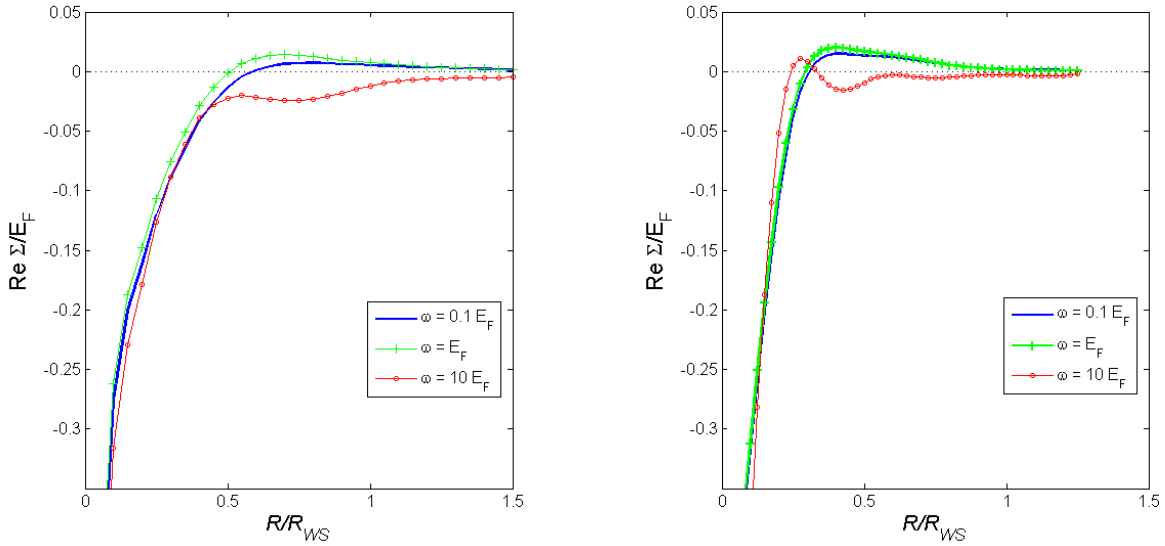

(a) $R_{\text{WS}} = 2$ (b) $R_{\text{WS}} = 4$

Figure 15: The frequency dependence of the total self-energy with $R_{\text{WS}} = 2$ and 4.

5 Conclusions

In this thesis work, the real space behavior of the self energy was investigated with the uniform electron gas model. The model was constructed with two typical electron density values. The self energy as a function of position was calculated with original codes under different frequencies and system densities. The results ware compared with the static COHSEX approximation. It can be concluded that

- Σ_{SEX} has a weak dependence on frequency whereas Σ_{COH} has a stronger dependence on frequency.
- Σ_{SEX} can surprisingly change sign and become positive.
- Σ_{SEX} is more localized than Σ_{COH}.
- Σ_{SEX} can be well approximated by a static screened exchange potential as well as an exchange potential with a Yukawa interaction characterized by the Fermi wave vector.
- Σ_{COH} is not as localized as the static COHSEX approximation would suggest, especially for high densities. However, both Σ_{SEX} and Σ_{COH} are still localized within the Wigner-Seitz radius even at high energy. The higher the energy the more localized the self-energy.
- Σ_{COH} shows more repulsive behavior at low density as a result of stronger correlation and displays a more pronounced oscillatory behaviour at high frequency.
- Σ is more localized the lower the density.

6 Outlook

As discussed in the previous sections, the static approximation for the screened-exchange term can simplify GW calculations and give rather accurate results. However, the Coulomb-hole term exhibits a more complex behavior and a simple approximation is still lacking. It is not surprising that even in the simplest uniform electron gas model, there are noticeable differences between the approximate values based on the static approximation and the exact ones. However, the localized behavior of the self-energy indicates the feasibility of finding a simple approximation for the Coulomb-hole term.

The same investigation can be carried out for real materials (metals, transition metal oxides, etc.) and the corresponding results can be compared with the electron gas results. A simple proposal to simplify the screened interaction is to adopt the local density approach as follows:

$$W(\boldsymbol{r},\boldsymbol{r'};\omega=0)=\frac{1}{2}\Big[W^0\big(\boldsymbol{r}-\boldsymbol{r'},\rho(\boldsymbol{r})\big)+W^0\big(\boldsymbol{r}-\boldsymbol{r'},\rho(\boldsymbol{r'})\big)\Big], \tag{6.1}$$

where W^0 is the electron gas screened interaction calculated in 3.2. If this approximation works well, it will reduce the computational effort greatly since computing the screened interaction is one of the bottle necks in GW calculations.

At present, when $\Sigma(\omega = E_F)$ of a certain material is of interest, the SEX part can be approximated with Σ^{Y}. The COH part, however, needs to be calculated directly. It would be ideal if Σ_{SEX} and Σ_{COH} could be modeled using the electron gas results. In the spirit of the local density approximation a simple model for the self-energy could be as follows:

$$\Sigma(\boldsymbol{r}, \boldsymbol{r'}; \omega = 0) = \frac{1}{2}\Big[\Sigma^0\big(\boldsymbol{r} - \boldsymbol{r'}, \rho(\boldsymbol{r})\big) + \Sigma^0\big(\boldsymbol{r} - \boldsymbol{r'}, \rho(\boldsymbol{r'})\big)\Big], \tag{6.2}$$

where Σ^0 is the self-energy of the homogeneous electron gas.

Acknowledgements

I would like to express my very great appreciation to Professor Ferdi Aryasetiawan for his valuable instructions and patient guidance. I would also like to extend my thanks to the LU Global Scholarship Committee for their kind support.

A The calculation of the self-energy under the GWA

In the frequency space, the GWA self-energy is given by,

$$\Sigma(\boldsymbol{r}, \boldsymbol{r'}; \omega) = i \int \frac{d\omega'}{2\pi} G(\boldsymbol{r}, \boldsymbol{r'}; \omega + \omega') W(\boldsymbol{r}, \boldsymbol{r'}; \omega'). \tag{A.1}$$

The exchange part of the self-energy is,

$$\Sigma_{\mathrm{X}}(\boldsymbol{r}, \boldsymbol{r'}; \omega) = i \int \frac{d\omega'}{2\pi} G(\boldsymbol{r}, \boldsymbol{r'}; \omega + \omega') v(\boldsymbol{r} - \boldsymbol{r'}) e^{i\eta\omega'}, \tag{A.2}$$

where the converging factor $e^{i\eta\omega'}$ represents that the equal time Green's function should be taken as $G(\boldsymbol{r}t, \boldsymbol{r'}t^+)$. With the spectral representation of the Green's function,

$$G(\boldsymbol{r}, \boldsymbol{r'}; \omega) = \int_{-\infty}^{\mu} d\omega' \frac{A(\boldsymbol{r}, \boldsymbol{r'}; \omega')}{\omega - \omega' - i\delta} + \int_{\mu}^{\infty} d\omega' \frac{A(\boldsymbol{r}, \boldsymbol{r'}; \omega')}{\omega - \omega' + i\delta}, \tag{A.3}$$

we have,

$$\begin{aligned} \Sigma_{\mathrm{X}}(\boldsymbol{r}, \boldsymbol{r'}; \omega) &= iv(\boldsymbol{r} - \boldsymbol{r'}) \int \frac{d\omega'}{2\pi} \\ &\times \left\{ \int_{-\infty}^{\mu} d\omega_1 \frac{A(\boldsymbol{r}, \boldsymbol{r'}; \omega_1)}{\omega + \omega' - \omega_1 - i\delta} + \int_{\mu}^{\infty} d\omega_1 \frac{A(\boldsymbol{r}, \boldsymbol{r'}; \omega_1)}{\omega + \omega' - \omega_1 + i\delta} \right\} e^{i\eta\omega'} \\ &= -v(\boldsymbol{r} - \boldsymbol{r'}) \int_{-\infty}^{\mu} d\omega_1 A(\boldsymbol{r}, \boldsymbol{r'}; \omega_1), \end{aligned} \tag{A.4}$$

where A is the spectral function. If the non-interacting spectral function is used,

$$A^0(\boldsymbol{r}, \boldsymbol{r'}; \omega) = \sum_k \psi_k(\boldsymbol{r}) \psi_k^*(\boldsymbol{r'}) \delta(\omega - \epsilon_k), \tag{A.5}$$

the exchange self-energy returns to the Fock exchange,

$$\Sigma_{\mathrm{X}}(\boldsymbol{r}, \boldsymbol{r'}) = -v(\boldsymbol{r} - \boldsymbol{r'}) \sum_k^{\mathrm{occ}} \psi_k(\boldsymbol{r}) \psi_k^*(\boldsymbol{r'}). \tag{A.6}$$

The correlation part of the screened interaction is defined as,

$$W_{\mathrm{c}} = W - v, \tag{A.7}$$

and it can be written in terms of its spectral representation,

$$W_{\mathrm{c}}(\boldsymbol{r}, \boldsymbol{r'}; \omega) = \int_{-\infty}^{0} d\omega_2 \frac{D(\boldsymbol{r}, \boldsymbol{r'}; \omega_2)}{\omega - \omega_2 - i\eta} + \int_{0}^{\infty} d\omega_2 \frac{D(\boldsymbol{r}, \boldsymbol{r'}; \omega_2)}{\omega - \omega_2 + i\eta}, \tag{A.8}$$

where

$$\begin{aligned} D(\boldsymbol{r}, \boldsymbol{r'}; \omega) &= -\frac{1}{\pi} \mathrm{sgn}(\omega) \mathrm{Im}\ W^c(\boldsymbol{r}, \boldsymbol{r'}; \omega) \\ &= -\frac{1}{\pi} \mathrm{sgn}(\omega) \mathrm{Im}\ W(\boldsymbol{r}, \boldsymbol{r'}; \omega). \end{aligned} \tag{A.9}$$

Combined with (A.3), the correlation part of the self-energy is,

$$\begin{aligned} \Sigma_{\mathrm{c}}(\boldsymbol{r}, \boldsymbol{r'}; \omega) = & i \int \frac{d\omega'}{2\pi} \int_{-\infty}^{\mu} d\omega_1 \int_{-\infty}^{0} d\omega_2 \frac{A(\boldsymbol{r}, \boldsymbol{r'}; \omega_1)}{\omega + \omega' - \omega_1 - i\delta} \times \frac{D(\boldsymbol{r}, \boldsymbol{r'}; \omega_2)}{\omega' - \omega_2 - i\eta} \\ & + i \int \frac{d\omega'}{2\pi} \int_{-\infty}^{\mu} d\omega_1 \int_{0}^{\infty} d\omega_2 \frac{A(\boldsymbol{r}, \boldsymbol{r'}; \omega_1)}{\omega + \omega' - \omega_1 - i\delta} \times \frac{D(\boldsymbol{r}, \boldsymbol{r'}; \omega_2)}{\omega' - \omega_2 + i\eta} \\ & + i \int \frac{d\omega'}{2\pi} \int_{\mu}^{\infty} d\omega_1 \int_{-\infty}^{0} d\omega_2 \frac{A(\boldsymbol{r}, \boldsymbol{r'}; \omega_1)}{\omega + \omega' - \omega_1 + i\delta} \times \frac{D(\boldsymbol{r}, \boldsymbol{r'}; \omega_2)}{\omega' - \omega_2 - i\eta} \\ & + i \int \frac{d\omega'}{2\pi} \int_{\mu}^{\infty} d\omega_1 \int_{0}^{\infty} d\omega_2 \frac{A(\boldsymbol{r}, \boldsymbol{r'}; \omega_1)}{\omega + \omega' - \omega_1 + i\delta} \times \frac{D(\boldsymbol{r}, \boldsymbol{r'}; \omega_2)}{\omega' - \omega_2 + i\eta}, \end{aligned} \tag{A.10}$$

where only the second and third terms in the right hand side are non-zero. With the symmetry,

$$D(\boldsymbol{r}, \boldsymbol{r'}; -\omega) = -D(\boldsymbol{r}, \boldsymbol{r'}; \omega), \tag{A.11}$$

(A.10) can be written as,

$$
\begin{aligned}
\Sigma_{\mathrm{c}}(\boldsymbol{r},\boldsymbol{r'};\omega) &= i\int\frac{d\omega'}{2\pi}\int_{-\infty}^{\mu}d\omega_1\int_0^{\infty}d\omega_2\frac{A(\boldsymbol{r},\boldsymbol{r'};\omega_1)}{\omega+\omega'-\omega_1-i\delta}\times\frac{D(\boldsymbol{r},\boldsymbol{r'};\omega_2)}{\omega'-\omega_2+i\eta}\\
&- i\int\frac{d\omega'}{2\pi}\int_{\mu}^{\infty}d\omega_1\int_0^{\infty}d\omega_2\frac{A(\boldsymbol{r},\boldsymbol{r'};\omega_1)}{\omega+\omega'-\omega_1+i\delta}\times\frac{D(\boldsymbol{r},\boldsymbol{r'};\omega_2)}{\omega'+\omega_2-i\eta}\\
&= \int_{-\infty}^{\mu}d\omega_1\int_0^{\infty}d\omega_2\frac{A(\boldsymbol{r},\boldsymbol{r'};\omega_1)D(\boldsymbol{r},\boldsymbol{r'};\omega_2)}{\omega+\omega_2-\omega_1-i\delta}\\
&+ \int_{\mu}^{\infty}d\omega_1\int_0^{\infty}d\omega_2\frac{A(\boldsymbol{r},\boldsymbol{r'};\omega_1)D(\boldsymbol{r},\boldsymbol{r'};\omega_2)}{\omega-\omega_2-\omega_1+i\delta}\\
&= \int_{-\infty}^{\infty}d\omega_1\theta(\mu-\omega_1)\int_{-\infty}^{\infty}d\omega_2\theta(\omega_2)\frac{A(\boldsymbol{r},\boldsymbol{r'};\omega_1)D(\boldsymbol{r},\boldsymbol{r'};\omega_2)}{\omega+\omega_2-\omega_1-i\delta}\\
&+ \int_{-\infty}^{\infty}d\omega_1\theta(\omega_1-\mu)\int_{-\infty}^{\infty}d\omega_2\theta(\omega_2)\frac{A(\boldsymbol{r},\boldsymbol{r'};\omega_1)D(\boldsymbol{r},\boldsymbol{r'};\omega_2)}{\omega-\omega_2-\omega_1+i\delta}.
\end{aligned}
\tag{A.12}
$$

With (A.5), we obtain,

$$
\begin{aligned}
\Sigma_{\mathrm{c}}(\boldsymbol{r},\boldsymbol{r'};\omega) &= \sum_k\theta(\mu-\epsilon_k)\int_{-\infty}^{\infty}d\omega_2\theta(\omega_2)\frac{\psi_k(\boldsymbol{r})\psi_k^*(\boldsymbol{r'})D(\boldsymbol{r},\boldsymbol{r'};\omega_2)}{\omega+\omega_2-\epsilon_k-i\delta}\\
&+ \sum_k\theta(\epsilon_k-\mu)\int_{-\infty}^{\infty}d\omega_2\theta(\omega_2)\frac{\psi_k(\boldsymbol{r})\psi_k^*(\boldsymbol{r'})D(\boldsymbol{r},\boldsymbol{r'};\omega_2)}{\omega-\omega_2-\epsilon_k+i\delta}.
\end{aligned}
\tag{A.13}
$$

The real part of the correlation self-energy is then,

$$
\begin{aligned}
\mathrm{Re}\ \Sigma_{\mathrm{c}}(\boldsymbol{r},\boldsymbol{r'};\omega) &= \sum_k\theta(\mu-\epsilon_k)\int_{-\infty}^{\infty}d\omega_2\theta(\omega_2)\frac{\psi_k(\boldsymbol{r})\psi_k^*(\boldsymbol{r'})D(\boldsymbol{r},\boldsymbol{r'};\omega_2)}{\omega+\omega_2-\epsilon_k}\\
&+ \sum_k\theta(\epsilon_k-\mu)\int_{-\infty}^{\infty}d\omega_2\theta(\omega_2)\frac{\psi_k(\boldsymbol{r})\psi_k^*(\boldsymbol{r'})D(\boldsymbol{r},\boldsymbol{r'};\omega_2)}{\omega-\omega_2-\epsilon_k}\\
&= \sum_k^{\mathrm{occ}}\psi_k(\boldsymbol{r})\psi_k^*(\boldsymbol{r'})\int_{-\infty}^{\infty}d\omega_2\frac{D(\boldsymbol{r},\boldsymbol{r'};\omega_2)}{\omega+\omega_2-\epsilon_k}\\
&- \sum_k^{\mathrm{occ}}\psi_k(\boldsymbol{r})\psi_k^*(\boldsymbol{r'})\int_{-\infty}^{0}d\omega_2\frac{D(\boldsymbol{r},\boldsymbol{r'};\omega_2)}{\omega+\omega_2-\epsilon_k}\\
&+ \sum_k^{\mathrm{unocc}}\psi_k(\boldsymbol{r})\psi_k^*(\boldsymbol{r'})\int_0^{\infty}d\omega_2\frac{D(\boldsymbol{r},\boldsymbol{r'};\omega_2)}{\omega-\omega_2-\epsilon_k}\\
&= -\sum_k^{\mathrm{occ}}\psi_k(\boldsymbol{r})\psi_k^*(\boldsymbol{r'})W_{\mathrm{c}}(\boldsymbol{r},\boldsymbol{r'};\epsilon_k-\omega)\\
&+ \sum_k\psi_k(\boldsymbol{r})\psi_k^*(\boldsymbol{r'})\int_0^{\infty}d\omega_2\frac{D(\boldsymbol{r},\boldsymbol{r'};\omega_2)}{\omega-\omega_2-\epsilon_k}.
\end{aligned}
\tag{A.14}
$$

Combining with the exchange part (A.6),

$$\begin{aligned}\text{Re } \Sigma(\boldsymbol{r}, \boldsymbol{r'}; \omega) = &- \sum_{k}^{\text{occ}} \psi_k(\boldsymbol{r}) \psi_k^*(\boldsymbol{r'}) W(\boldsymbol{r}, \boldsymbol{r'}; \epsilon_k - \omega) \\ &+ \sum_k \psi_k(\boldsymbol{r}) \psi_k^*(\boldsymbol{r'}) \int_0^\infty d\omega_2 \frac{D(\boldsymbol{r}, \boldsymbol{r'}; \omega_2)}{\omega - \omega_2 - \epsilon_k}.\end{aligned} \tag{A.15}$$

Under the static approximation $\omega - \epsilon_k \approx 0$, the first term in the right hand side of (A.15) becomes,

$$\text{Re } \Sigma_{\text{SEX}}^{\text{static}}(\boldsymbol{r}, \boldsymbol{r'}) = - \sum_{k}^{\text{occ}} \psi_k(\boldsymbol{r}) \psi_k^*(\boldsymbol{r'}) W(\boldsymbol{r}, \boldsymbol{r'}; 0), \tag{A.16}$$

and the second term in the right hand side of (A.15) becomes,

$$\begin{aligned}\text{Re } \Sigma_{\text{COH}}^{\text{static}}(\boldsymbol{r}, \boldsymbol{r'}) &= \frac{1}{\pi} \sum_k \psi_k(\boldsymbol{r}) \psi_k^*(\boldsymbol{r'}) \int_0^\infty d\omega_2 \frac{\text{Im } W_{\text{c}}(\boldsymbol{r}, \boldsymbol{r'}; \omega_2)}{\omega_2} \\ &= \frac{1}{2} \delta(\boldsymbol{r} - \boldsymbol{r'}) \int_{-\infty}^\infty d\omega_2 \frac{D(\boldsymbol{r}, \boldsymbol{r'}; 0)}{0 - \omega_2} \\ &= \frac{1}{2} \delta(\boldsymbol{r} - \boldsymbol{r'}) W_{\text{c}}(\boldsymbol{r}, \boldsymbol{r'}; 0).\end{aligned} \tag{A.17}$$

References

[1] Douglas R Hartree. The wave mechanics of an atom with a non-Coulomb central field. Part I. Theory and methods. In *Mathematical Proceedings of the Cambridge Philosophical Society*, volume 24, pages 89–110. Cambridge University Press, 1928.

[2] Vladimir Fock. Näherungsmethode zur Lösung des quantenmechanischen Mehrkörperproblems. *Zeitschrift für Physik*, 61(1-2):126–148, 1930.

[3] John Clarke Slater. *The self-consistent field for molecules and solids (Quantum Theory of Molecules and Solids)*, volume 4. McGraw-Hill, 1974.

[4] Pierre Hohenberg and Walter Kohn. Inhomogeneous electron gas. *Physical Review*, 136(3B):B864, 1964.

[5] Walter Kohn and Lu Jeu Sham. Self-consistent equations including exchange and correlation effects. *Physical Review*, 140(4A):A1133, 1965.

[6] Eberhard KU Gross and Reiner M Dreizler. *Density functional theory*, volume 337. Springer Science & Business Media, 2013.

[7] Lars Hedin. New method for calculating the one-particle Green's function with application to the electron-gas problem. *Physical Review*, 139(3A):A796, 1965.

[8] Ferdi Aryasetiawan and Olle Gunnarsson. The GW method. *Reports on Progress in Physics*, 61(3):237, 1998.

[9] Neil W. Ashcroft and N. David Mermin. *Solid state physics*. Holt, Rinehart and Winston, New York, 1976.

[10] Mark van Schilfgaarde, Takao Kotani, and Sergey Faleev. Quasiparticle self-consistent GW theory. *Physical Review Letters*, 96(22):226402, 2006.

[11] Alexander L Fetter and John Dirk Walecka. *Quantum theory of many-particle systems*. Courier Corporation, 2012.

[12] Milton Abramowitz and Irene A Stegun. *Handbook of mathematical functions: with formulas, graphs, and mathematical tables*, volume 55. Courier Corporation, 1964.

[13] Lars Hedin and S S Lundqvist. *Solid State Physics*, volume 23. F Seitz D Turnbull and H Ehrenreich (New York: Academic), 1969.